# ORIGINAL RESEARCH

Divergent Roles of Kupffer Cell TLR2/3 Signaling in Alcoholic Liver Disease and the Protective Role of EGCG

Pingping Luo,[1,2,*] Fei Wang,[3,*] Nai-Kei Wong,[4] Yi Lv,[2] Xinxin Li,[5] Mianhuan Li,[1,2] George L. Tipoe,[6] Kwok-Fai So,[7] Aimin Xu,[8] Shuaiyin Chen,[9] Jia Xiao,[1,2,6,§] and Hua Wang[10,§]

[1]Clinical Medicine Research Institute, First Affiliated Hospital of Jinan University, Guangzhou, China; [2]Laboratory of Neuroendocrinology, School of Biological Sciences, Fujian Normal University, Fuzhou, China; [3]Digestive Disease Institute of Tongji Hospital, Tongji University School of Medicine, Shanghai, China; [4]State Key Discipline of Infectious Diseases, Department of Infectious Diseases, Shenzhen Third People's Hospital, Southern University of Science and Technology, Shenzhen, China; [5]Research Center for Clinical Sciences, Second Affiliated Hospital, Zhejiang University School of Medicine, Hangzhou, China; [6]School of Biomedical Sciences, Li Ka Shing Faculty of Medicine, University of Hong Kong, Hong Kong; [7]GMH Institute of CNS Regeneration, Guangdong Medical Key Laboratory of Brain Function and Diseases, Jinan University, Guangzhou, China; [8]Department of Medicine, Li Ka Shing Faculty of Medicine, University of Hong Kong, Hong Kong; [9]Department of Epidemiology, College of Public Health, Zhengzhou University, Zhengzhou, China; and [10]Department of Oncology, The First Affiliated Hospital, Institute for Liver Diseases of Anhui Medical University, Hefei, China
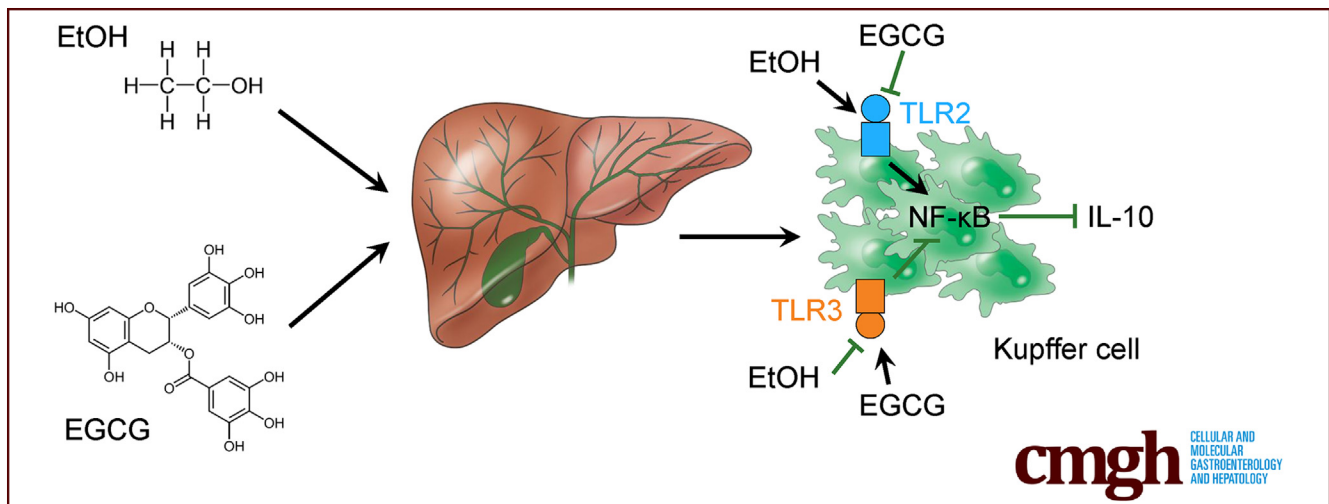
SUMMARY

Alcoholic liver disease affects millions worldwide. We found that epigallocatechin-3-gallate from green tea directly interacts with hepatic Kupffer cell Toll-like receptor 2/3 receptors and modulates downstream interleukin-10 signaling to exert divergent effects on ethanol-induced liver injury.

BACKGROUND & AIMS: Toll-like receptor 2 (TLR2) and TLR3 regulate hepatic immunity under pathological conditions, but their functions and potential drug targets in alcoholic liver disease (ALD) remain poorly understood.

METHODS: ALD-associated liver injury were induced in *TLR2* knockout (*TLR2^{-/-}*), *TLR3^{-/-}*, *TLR2^{-/-}* bone marrow transplanted (BMT), *TLR3^{-/-}* BMT, *IL-10^{-/-}* mice, and their wild-type littermates through ethanol challenge with or without co-administered epigallocatechin-3-gallate (EGCG). Moreover, Kupffer cells were depleted by GdCl₃ injection to evaluate their pathogenic roles in ALD.

RESULTS: We identified that deficiency of *TLR2* and *TLR3* significantly alleviated and aggravated ALD-induced liver injury, respectively. Mechanistically, Kupffer cell inactivation, M1 to M2 polarization, and IL-10 production via STAT3 activation contributed to hepatic protection mediated by concurrent TLR2 inhibition and TLR3 agonism. These findings were further confirmed in *TLR2* and *TLR3* BMT mice. We also identified a novel ALD-protective agent EGCG which directly interacted with Kupffer cell TLR2/3 to induce IL-10 production. Deficiency of *IL-10* aggravated ALD injury and blunted EGCG-mediated hepatoprotection while depletion of Kupffer cells partially recovered liver injury but abolished EGCG's actions.

CONCLUSIONS: Altogether, our results illustrate the divergent roles of Kupffer cells TLR2/3 in ALD progression via anti-inflammatory cytokine IL-10 production. *(Cell Mol Gastroenterol Hepatol 2020;9:145–160; https://doi.org/10.1016/j.jcmgh.2019.09.002)*

Keywords: Alcoholic Liver Disease; Kupffer Cell; Toll-like Receptor; EGCG.

See editorial on page 187.

Alcoholic liver disease (ALD) encompasses a broad spectrum of disorders including steatosis, steatohepatitis, fibrosis, cirrhosis, and hepatocellular carcinoma. Despite the growing social impact and disease burden of ALD worldwide, disproportionately few advances have been seen in the management of this disease.[1] To date, alcohol abstinence is the primary and most efficacious self-administered therapy for ALD, with no specific drug or therapy being approved by Food and Drug Administration. Clinical evidence suggests that corticosteroids therapy remains the best available option to complement abstinence, as it allows modest though significant improvement in short-term mortality for severe alcoholic hepatitis.[2] Unfortunately, the adverse effects of corticosteroids are also evident, which include increased infection risks and gastrointestinal hemorrhage. On the other hand, auxiliary nutritional treatments such as N-acetyl-cysteine (NAC) and vitamins have also been recommended for clinical ALD therapy for the purpose of improving hepatic injury and mortality.[3,4]

Given the potential therapeutic implications, involvement of Toll-like receptors (TLRs) in liver diseases has galvanized much interest over the last decade.[5] Ingestion of ethanol disrupts intestinal integrity and induces migration of gut-derived microbial products (eg, lipopolysaccharide [LPS]) through portal circulation reaching the liver. LPS activates TLR4 in Kupffer cells to produce proinflammatory cytokines (eg, tumor necrosis factors), which in turn, lead to a cascade of release of other proinflammatory cytokines and chemokines to provoke alcoholic steatohepatitis.[6,7] It has been shown that enteral ethanol exposure induced hepatic *TLR2* messenger RNA expression, which was inhibited by diphenyleneiodonium sulfate injection.[8] Interestingly, contradictory results of TLR2 deficiency in ALD have been reported. One study found that TLR2 deficiency did not significantly influence hepatic damages after ethanol administration,[9] while the other demonstrated that $Tlr2^{-/-}$ mice are resistant to the chronic ethanol-feeding model.[10] In contrast, it was reported that activation of TLR3 attenuated ALD by stimulating Kupffer cells and stellate cells through interleukin (IL)-10 production.[11] However, whether TLR2/3 in Kupffer cells constitute bona fide therapeutic targets remains unknown.

Emerging evidence has illuminated the evolving roles of green tea from a simple herbal beverage to a novel source of natural products with hepatoprotective functions. We and other research groups have revealed the ameliorative effects of green tea extract or polyphenol epigallocatechin-3-gallate (EGCG) on nonalcoholic fatty liver disease–associated hepatic injury, which are generally achieved through mitigation of hepatic steatosis, inflammation, oxidative stress, and cell death.[12–14] Although several studies have found that green tea extract protected mice liver from ALD-associated liver damage by inhibition of alcohol absorption or reduction of hepatic inflammation/oxidative stress, little is known about whether and how EGCG alleviates ALD symptoms in vivo.[15,16] Of particular import, the direct regulatory targets of EGCG in ALD development remain to be identified. In this study, we interrogated the hepatoprotective effects of EGCG in a chronic-binge murine ALD model (the NIAAA model) in comparison with other commonly used ALD chemotherapeutic agents. The direct interactions between EGCG and TLR2/3 were established and the receptors' apparently opposite regulatory roles were elucidated by using $Tlr2^{-/-}$ and $Tlr3^{-/-}$ animals, and bone marrow–transplanted (BMT) *Tlr2* or *Tlr3* mice. We demonstrated that EGCG is a highly potent and safe agent for daily supplementation of ALD therapy, whose pharmacological benefits seem sustained via inhibition of TLR2 and stimulation of TLR3 in Kupffer cells.

Results

EGCG Mitigates ALD-Associated Liver Injury

In contrast to pair-fed mice, mice subjected to chronic ethanol challenge showed leveling body weight change. Administration of EGCG restored mouse body weight without influencing the food intake (Figure 1A). As expected, development of ALD caused typical injuries, including significantly increased serum aminotransferase levels, triglyceride (TG) level, total cholesterol (TC) level (Figure 1B), serum proinflammatory cytokine (tumor necrosis factor alpha [TNF-α], interleukin [IL]-1β, IL-6), chemokine (MCP-1), and anti-inflammatory cytokine (IL-10) levels (Figure 1C). In the liver, lipid droplet accumulation and inflammatory cell infiltration was observed in the ethanol-fed mice. Hepatic TG level was also significantly elevated in the ALD mice (Figure 1D). Co-treatment with EGCG effectively ameliorated all the ALD phenotypes without affecting the healthy mice, except that it further enhanced the serum level of anti-inflammatory IL-10 (Figure 1B–D). In addition, when compared with the ALD groups, treatment with EGCG reduced the lipid-synthesis marker protein expression (sterol regulatory element-binding protein 1c and fatty acid synthase), and the phosphorylated level of nuclear factor kappa B (NF-κB) p65. In contrast, phosphorylated adenosine 5′-monophosphate–activated protein kinase (AMPK) and signal transducer and activator of transcription 3 (STAT3) was further activated by the EGCG treatment (Figure 1E). Importantly, vehicle-EGCG administration did not result in
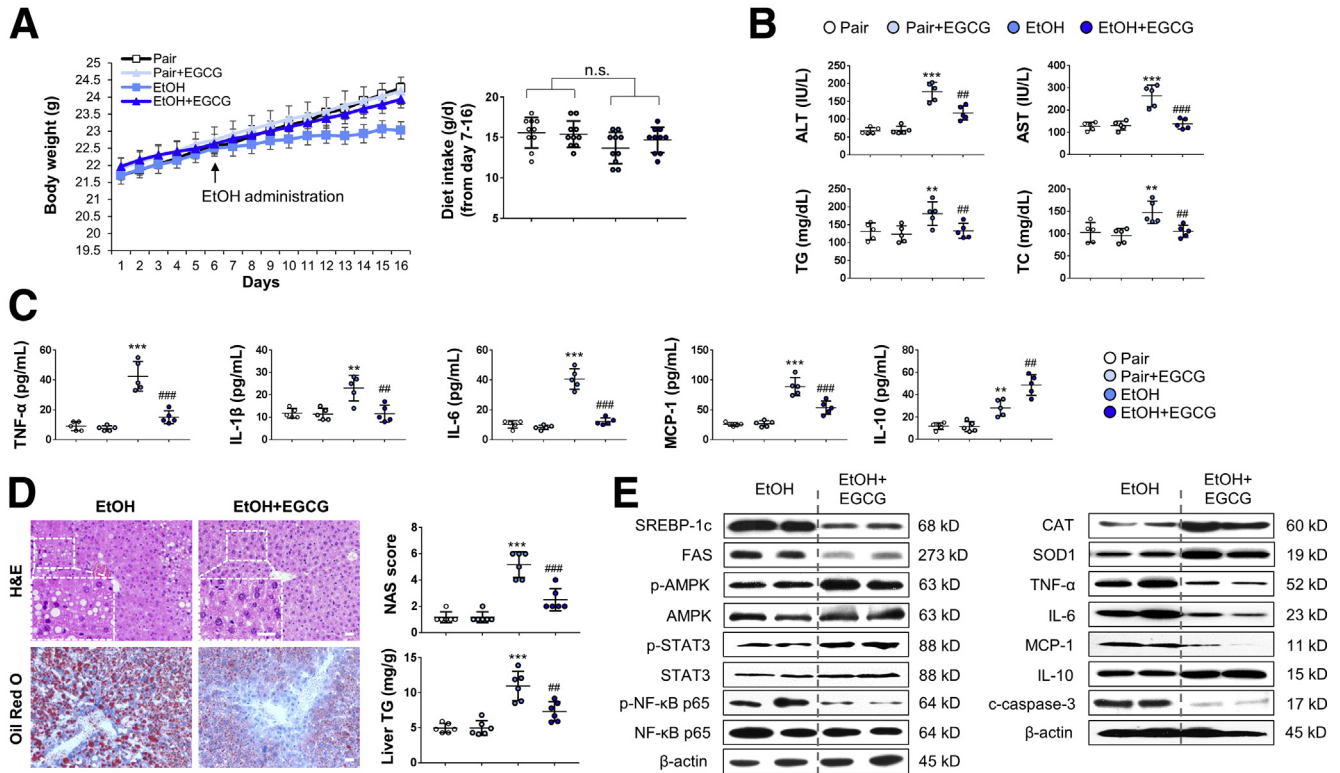
🔲 **Most current article**

Figure 1. EGCG improves ALD-associated liver injury without influencing food intake. (*A*) Body weight and dietary intake changes of mice fed with control diet or ethanol diet (chronic-binge ALD model), in the presence or absence of daily EGCG gavage (n = 10) (Two independently repeated experiments with similar results). (*B*) Serum biochemistry for ALT, AST, TG, and TC (n = 5). (*C*) Serum levels of cytokines and chemokines measured by using enzyme-linked immunosorbent assay (n = 5). (*D*) Histology (HE and Oil Red O staining) and corresponding NAS score and liver TG changes of all groups of mice (n = 6). (*E*) Whole liver tissue immunoblotting results. Values are expressed as mean ± SD (3 independently repeated experiments with similar results). **, ***$P < .01, 0.001$ against pair group; ##, ###$P < .01, 0.001$ against EtOH group. Scale bar = 20 μm. Statistical comparisons between groups were done by using the Kruskal-Wallis test followed by Dunn's post hoc test to detect differences in all groups. n.s., not significant

any adverse effects on all the parameters we measured, suggesting that the compound has very low or negligible toxicity as a treatment in ALD. Next, to test whether EGCG is superior to other well-documented hepatoprotective agents in improving ALD-associated hepatic injury, we co-treated ethanol-fed mice with resveratrol, silibinin, NAC, or prednisolone. It was found that EGCG, resveratrol, silibinin, and NAC significantly ameliorated ethanol-induced hepatic histological abnormalities, hepatic TG elevation, and serum aminotransferase enhancement, in which EGCG had the best improving functions. Unexpectedly, despite being a recommended drug for acute alcoholic steatohepatitis treatment clinically, prednisolone co-treatment had no effect on ALD in this murine model (Figure 2).

EGCG Reduces Macrophage Activation and Infiltration

FACS analysis of the mice liver showed that when compared with the ALD group, co-treatment with EGCG significantly decreased F4/80$^+$ CD11b$^+$ cells, while the numbers of natural killer cells and natural killer T cells were improved. No significant change of other cell types (ie, T cells

and granulocytes) were observed between these 2 groups (Figure 3*A*, Table 2). In immunohistochemistry analysis, fewer infiltrating F4/80$^+$ cells in the liver tissue were observed in EtOH+EGCG co-treatment group compared with the ethanol group (Figure 3*B*). In Kupffer cells isolated from the mice liver, EGCG enhanced the phosphorylation of extracellular signal-regulated kinase (ERK) but inhibited p38 mitogen-activated protein kinase (MAPK) and NF-κB p65 phosphorylation (Figure 3*C*). Also, EGCG suppressed the messenger RNA expression levels of proinflammatory cytokine and chemokine (TNF-α and IL-6) but further enhanced the level of anti-inflammatory cytokine (IL-10) in Kupffer cells (Figure 3*D*). The cell apoptosis of Kupffer cells was also suppressed by EGCG (Figure 3*E*). Next, we tested the hypothesis that EGCG could directly induce IL-10 production from Kupffer cells, both under resting and injury conditions. In freshly prepared Kupffer cells from healthy mice, EGCG significantly increased IL-10 levels at both transcriptional and translational levels following 8 hours incubation of the compound (Figure 3*F*). Immunofluorescence assay of IL-10 further corroborated this result in Kupffer cells (Figure 3*G*). In vitro challenge with LPS in freshly isolated Kupffer cells significantly elevated the phosphorylated levels of p38
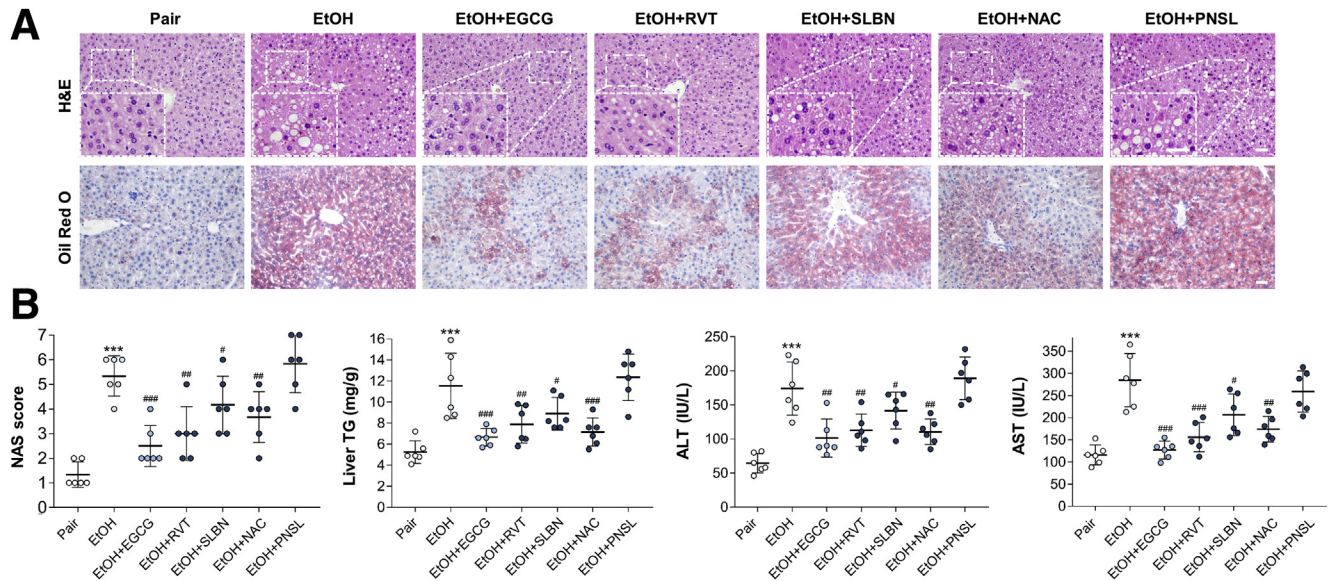
Figure 2. EGCG exhibits superior ameliorative effects on ALD-induced to other commonly used hepatoprotective agents, including resveratrol (RVT), silibinin (SLBN), N-acetyl-L-cysteine NAC, and prednisolone (PNSL). (A) Representative hepatic H&E/Oil Red O results. (B) Results of NAS and serum chemistry, including liver TG, ALT, and AST. Values are expressed as mean ± SD (6 mice per group, 3 independently repeated experiments with similar results). ***$P < .001$ against pair group; #, ##, ###$P < .05$, .01, and .001 against EtOH (ALD) group. Scale bar = 20 μm. Statistical comparisons between groups were done by using the Kruskal-Wallis test followed by Dunn's post hoc test to detect differences in all groups.

MAPK, ERK, and NF-κB p65 in a time-dependent manner. In agreement with the in vivo alterations, addition of EGCG inhibited p38 MAPK and NF-κB p65 phosphorylation but further promoted ERK phosphorylation (Figure 3H).

EGCG Promotes Kupffer Cell M2 Polarization

Inhibition of Kupffer cell M2-to-M1 polarization has proved to be effective in retarding ALD progression.[17] To test whether EGCG possesses similar function, we first measured the messenger RNA changes of M1 polarization markers (*iNOS* and *CXCL9-11*) and M2 polarization markers (*Arg1*, *Retnla*, *Mrc1*, and *Chi3l3*) in Kupffer cells isolated from treated mice. Our results showed that ethanol consumption significantly increased both M1- and M2-polarization of Kupffer cells. Coadministration of EGCG suppressed M1-polarization markers' expression but further promoted the level of M2-polarization markers (Figure 4A and B). Strikingly, changes of serum alanine aminotransferase (ALT), aspartate aminotransferase (AST), TG, and TC were strongly associated with the Kupffer cell M2/M1 ratio (Figure 4C). Consistent with results of the in vivo model, conditioned medium from LPS-stimulated M1-polarized Kupffer cells promoted primary hepatocyte steatosis and NF-κB p65 expression, whereas IL-4–stimulated M2-polarized conditioned medium had little effect (Figure 4D). To further prove the effect of EGCG on M2-polarization, double immunofluorescence for the macrophage marker F4/80 and for either the M1 marker inducible nitric oxide synthase (iNOS) or the M2 marker CD206 was applied to characterize cultured primary Kupffer cells from healthy mice. F4/80$^+$ cells without iNOS

and CD206 co-staining was classified as M0 phenotype. In vitro ethanol incubation caused a slight drop in the total number of Kupffer cells, as assessed by F4/80 immunostaining. Ethanol drastically reduced M0 density but promoted M1 polarization. The density of M2-polarized cells was not significantly changed. In the EGCG co-treated group, both densities of M2-polarized and M0 cells were recovered (Figure 4E). The M2/M1 ratio of Kupffer cells were positively associated with the production of IL-10 (Figure 4F).

EGCG Directly Targets TLR2/3 on Kupffer Cells to Induce IL-10 Production

Activated Kupffer cells play a major role in promoting ALD progression, in part via signaling of different TLRs. To clarify the direct targets of EGCG on Kupffer cells, biophysical assays including surface plasmon resonance (SPR) and thermal shift assay were conducted to test for possible direct interactions between EGCG and TLR2/3/4/9. It was found that the interaction between EGCG and TLR2 was relatively strong, whereas the interaction between EGCG and TLR3 was intermediate. Both TLR4 and TLR9 had very weak interactions with EGCG (Figure 5A). The docking results indicated that EGCG forms numerous of hydrogen bonds with TLR3 and double-strand RNA, such as interact with residues of Lys-493, Asn-494, Val-495, Asp-496, Asn-516, Asn-520 in TLR3, and U-27, G-28 in double-strand RNA. Structurally, these results suggested that EGCG may strengthen the interaction between TLR3 and double-strand RNA (Figure 5B). When *Tlr2* and *Tlr3* were knocked out, the direct stimulatory effects of EGCG on
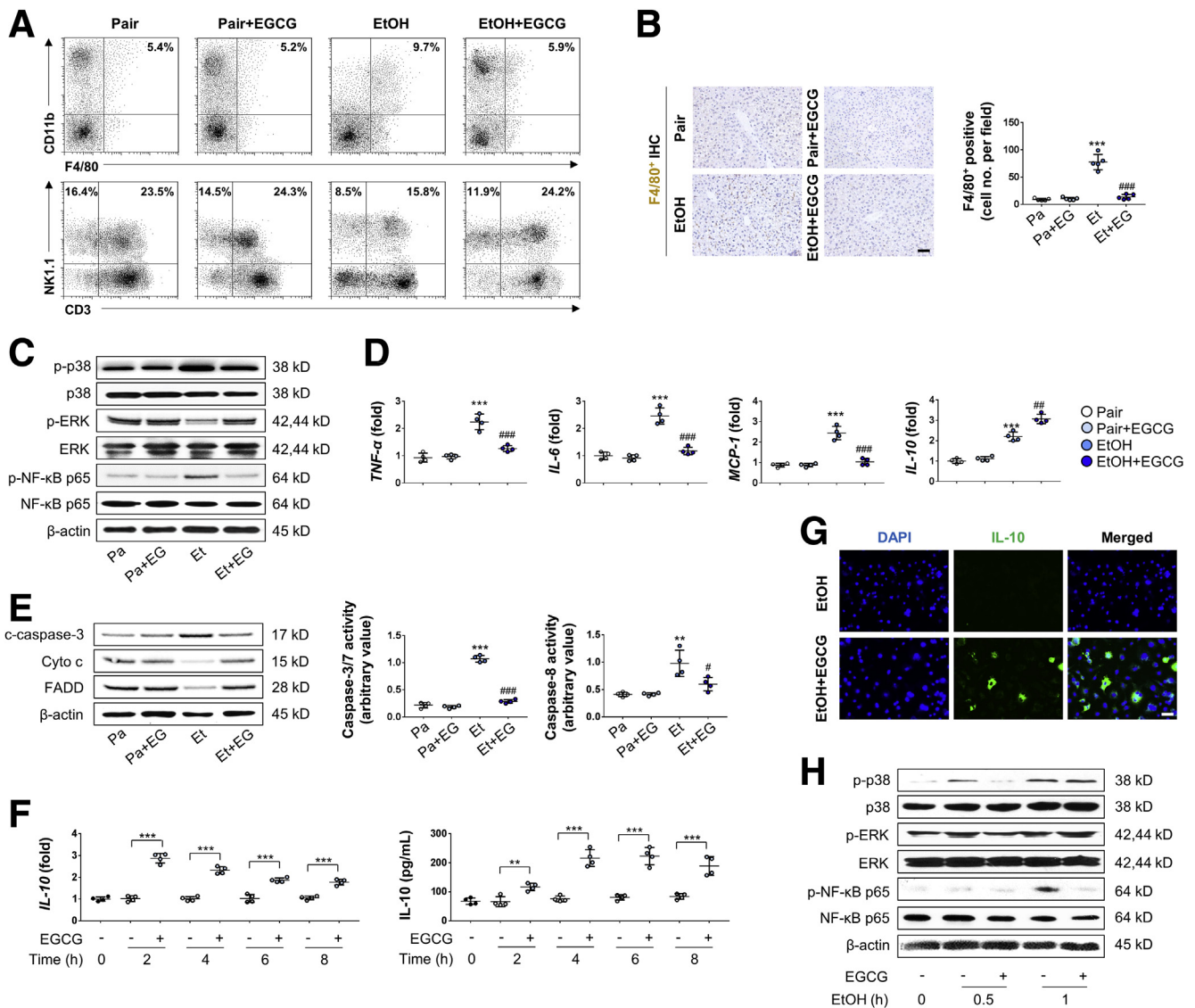
Figure 3. EGCG inhibited macrophage activation, Kupffer cell infiltration and apoptosis induced by ethanol diet. (*A*) Liver MNC composition changes (macrophages, natural killer cells, and natural killer T cells) were measured by FACS (representative FACS data). (*B*) Representative hepatic F4/80$^+$ cell staining and corresponding quantification from pair mice or mice treated with ethanol diet or EGCG (n = 5; scale bar = 20 μm). (*C*) Whole-liver tissue immunoblotting results (Pa, Pair; Pa+EG, Pair+EGCG; Et, EtOH; Et+EG, EtOH+EGCG). (*D*) Kupffer cell messenger RNA changes of cytokines and chemokines from the mice liver (n = 4). (*E*) Changes of caspase-3/7/8 activity and protein marker of cell apoptosis of isolated Kupffer cells in all groups (n = 4). (*F*) Expressional changes of IL-10 from isolated Kupffer cells with or without 50 μg/mL EGCG co-incubation at both the transcriptional and translational levels (n = 4). (*G*) Cultured Kupffer cells were treated with 200-mM EtOH or 50-μg/mL EGCG for 2 hours, then stained with IL-10 antibody and DAPI (representative images; scale bar = 50 μm). (*H*) Immunoblot results of MAPK markers and NF-κB p65 from cultured Kupffer cells. Cells were pretreated with or without 50-μg/mL EGCG for 30 minutes, then further treated with 200-mM ethanol for 0.5 or 1 hour. Values are expressed as mean ± SD (3 independently repeated experiments with similar results). **, ***P < .01, 0.001 against pair group; #, ###P < .05, 0.001 against EtOH (ALD) group. For panel *F*: **, ***P < .01, 0.001 between indicated groups.

in vitro IL-10 production were partially and totally abolished in cultured *Tlr2*$^{-/-}$ and *Tlr3*$^{-/-}$ Kupffer cells, respectively (Figure 5*C*). Consistently, the modulatory effects of EGCG on MAPK and NF-κB p65 phosphorylation were also significantly impaired by *Tlr2* or *Tlr3* deficiency (Figure 5*D*). When primary hepatocytes were cultured with conditioned medium from ethanol-stimulated *Tlr2*$^{-/-}$ Kupffer cells, hepatocyte steatosis and NF-κB p65

activation were both attenuated. Parallel experiments using conditioned medium from ethanol-stimulated *Tlr3*$^{-/-}$ Kupffer cells gave opposite results (Figure 5*E*). Interestingly, EGCG-mediated cell protection in *Tlr3*$^{-/-}$ Kupffer cells conditioned medium-treated hepatocytes were impaired (Figure 5*E*). Collectively, we identified that EGCG directly interacted with TLR2/3 on Kupffer cells to induce IL-10 production.
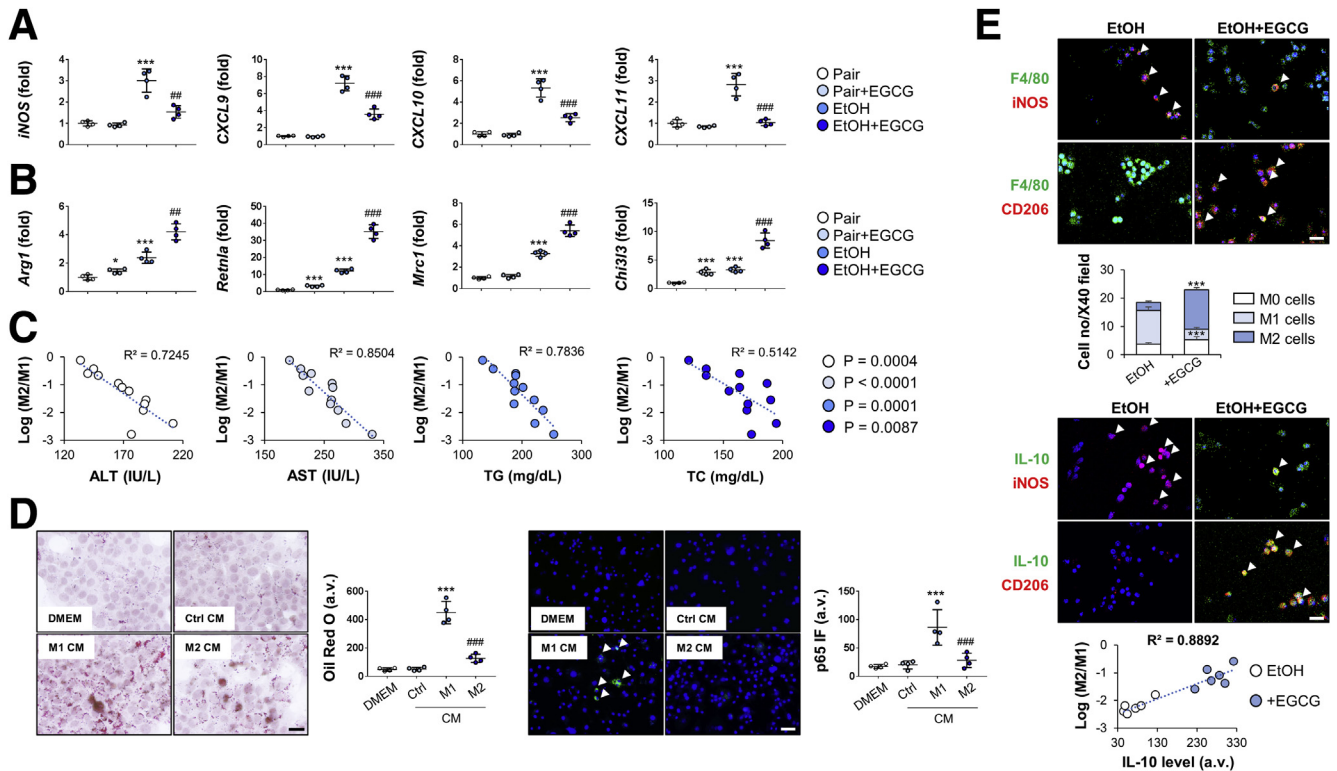
Figure 4. EGCG promotes M1 to M2 polarization of Kupffer cells. (*A*, *B*) Real-time PCR results of M1 and M2 key markers' expression changes of Kupffer cells isolated from mice treated with ethanol diet or EGCG co-consumption (n = 4). (*C*) Correlation analysis between Kupffer cell polarization and serum chemistry (ALT, AST, TG, and TC). (*D*) Representative Oil Red O staining and NF-κB p65 immunofluorescence of mouse hepatocyte AML-12 treated with conditioned medium from LPS (M1)- or IL-4 (M2)–stimulated isolated primary Kupffer cells (n = 4). (*E*) Double staining analysis of cultured Kupffer cells with F4/80, iNOS (M1 marker), CD206, and IL-10. Macrophages were classified as M0 (F4/80$^+$, iNOS$^-$, CD206$^-$), M1 (F4/80$^+$, iNOS$^+$, CD206$^-$), and M2 (F4/80$^+$, iNOS$^-$, CD206$^+$). Correlation between IL-10 production and macrophage polarization was analyzed. Values are expressed as mean $\pm$ SD (Three independently repeated experiments with similar results). *, **, ***$P < .05$, .01, and .001 against pair group; ##, ###$P < .01$, 0.001 against EtOH (ALD) group. Scale bar = 50 μm. Statistical comparisons between groups were done by using the Kruskal-Wallis test followed by Dunn's post hoc test to detect differences in all groups.

Kupffer Cell TLR2 and TLR3 Play Diverse Roles in ALD Progression and EGCG Protection Through IL-10

To further dissect the roles of TLR2 and TLR3 in ALD progression and EGCG protection, we induced ALD in *Tlr2*$^{-/-}$ and *Tlr3*$^{-/-}$ mice in the absence or presence of EGCG co-treatment. Results of serum aminotransferase level, hepatic histology, serum TNF-α/IL-10 protein level, and hepatic F4/80$^+$ cell infiltration suggested that deficiency of *Tlr2* effectively alleviated ALD-induced injury while *Tlr3* deficiency aggravated such injury (Figure 6*A–D*). Moreover, the hepatic regulatory effects of EGCG on lipid metabolism, AMPK, and NF-κB p65 pathway markers expression in the ALD mice were markedly disrupted by the deficiency of *Tlr2* or *Tlr3* (Figure 6*E*). In Kupffer cells, *Tlr2* knockout (KO) not only promoted the basal M2/M1 ratio, but also potentiated the M2-polarization mediated by EGCG. In contrast, addition of EGCG did not promote the M2-polarization of Kupffer cells in *Tlr3* KO mice (Figure 6*F*).

We then transplanted bone marrow from wild-type (WT), *Tlr2*$^{-/-}$, or *Tlr3*$^{-/-}$ mice into healthy WT mice to further investigate whether the regulatory effects of TLR2

and TLR3 on ALD progression were, at least partially, Kupffer cell–specific. As we expected, after the induction of ALD, *Tlr2*$^{-/-}$ BMT mice showed alleviated injuries, whereas *Tlr3*$^{-/-}$ BMT mice had exacerbated injuries, as evidenced by the changes in serum aminotransferase levels, liver histology, serum TNF-α/IL-10 level, and F4/80$^+$ infiltration in the liver compared with that of the WT littermates (Figure 7*A–D*). In agreement with results for the *Tlr2* and *Tlr3* KO mice, supplementation of EGCG had little effects on MAPK and NF-κB p65 phosphorylation regulation (Figure 7*E*) and M1-to-M2 promotion in *Tlr2* and *Tlr3* BMT mice (Figure 7*F*).

To validate whether the beneficial effects of EGCG and TLR3 were largely depended on IL-10 production, we repeated the ALD damage experiments in the absence or presence of EGCG co-consumption in *IL-10*$^{-/-}$ mice. Mice with *IL-10* deficiency exhibited more profound phenotypes of liver injury (eg, serum aminotransferases, hepatic histology, lipogenesis, Kupffer cell infiltration, inflammation), indicating an essential protective role of IL-10 during ALD development. EGCG consumption, however, showed blunted protective effects on these abnormalities when *IL-10* was knocked out (Figure 8).
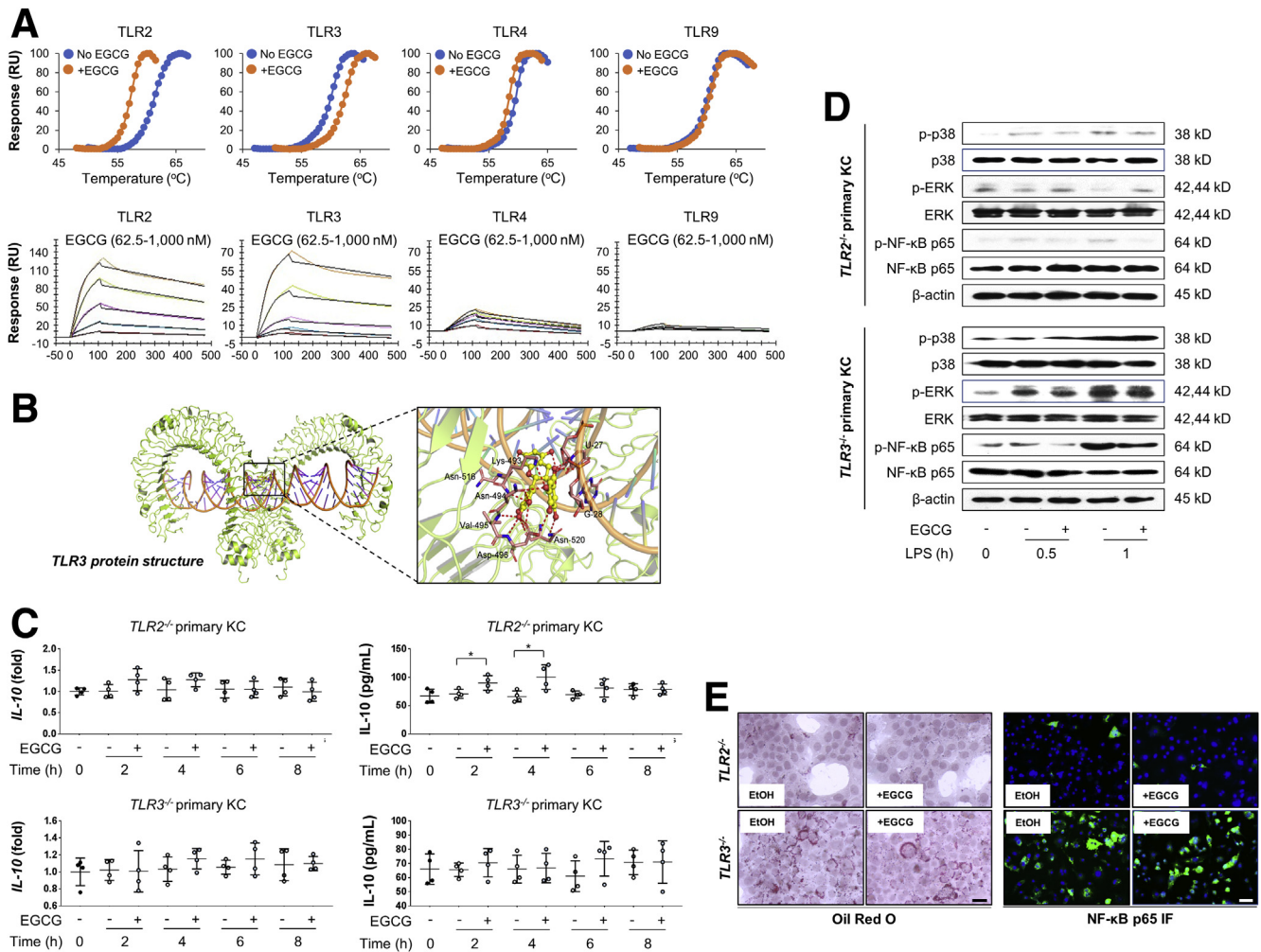
Figure 5. TLR2 and TLR3 are the direct regulatory targets of EGCG. (*A*) Thermal shift assay results of TLR2/3/4/9 in the presence or absence of EGCG, and SPR results of the direct interaction between TLR2/3/4/9 and 62.5–1000 nM EGCG. (*B*) The proposed complex of EGCG with the ligand-binding pocket of TLR3. The ribbon structure displays the predicted bonds between EGCG and TLR3. (C) Expressional changes of IL-10 from isolated Kupffer cells from $Tlr2^{-/-}$ and $Tlr3^{-/-}$ mice with or without 50-μg/mL EGCG co-incubation at both transcriptional and translational levels (n = 4). (*D*) Cultured Kupffer cells from $Tlr2^{-/-}$ and $Tlr3^{-/-}$ mice were pretreated with or without 50 μg/mL EGCG for 30 minutes, then further treated with 200 mM LPS for 0.5 or 1 hour. Key protein markers were subjected to immunoblotting. (*E*) Representative Oil Red O staining and NF-κB p65 immunofluorescence of mouse hepatocyte AML-12 treated with conditioned medium from EtOH or EGCG treated Kupffer cells from $Tlr2^{-/-}$ and $Tlr3^{-/-}$ mice. Values are expressed as mean $\pm$ SD (3 independently repeated experiments with similar results). **$P < .01$. Statistical comparisons between groups were done by using the Kruskal-Wallis test followed by Dunn's post hoc test to detect differences in all groups.

Lastly, to further verify the function of Kupffer cells during ALD progression, GdCl$_3$ was used to deplete Kupffer cells during the establishment of ALD injury in WT mice. One-week injection of GdCl$_3$ successfully reduced the hepatic expression of macrophage markers (F4/80 and CD68) (Figure 9). When ALD was induced, depletion of Kupffer cells in mice significantly ameliorated serum levels of aminotransferase, proinflammatory cytokine, and chemokine, as well as improved hepatic histology and lipogenesis. The hepatoprotective effects of EGCG were also drastically diminished by the depletion of Kupffer cells (Figure 9). Collectively, our data demonstrated that Kupffer cells were indispensable for ALD progression. As direct targets of EGCG, TLR2 and TLR3 mediated opposite regulatory effects on hepatic IL-10 production.

Discussion

ALD is recognized as a notable disease burden in most World Health Organization (WHO) member countries. Kupffer cell dysfunction has been strongly implicated in the pathogenesis of ALD though its molecular underpinnings are not fully understood. Herein, we used biophysical and BMT methods coupled to transgenic approaches to clarify the roles of distinct Kupffer cell TLRs in a mouse model of chronic plus binge ethanol consumption. Intriguingly,
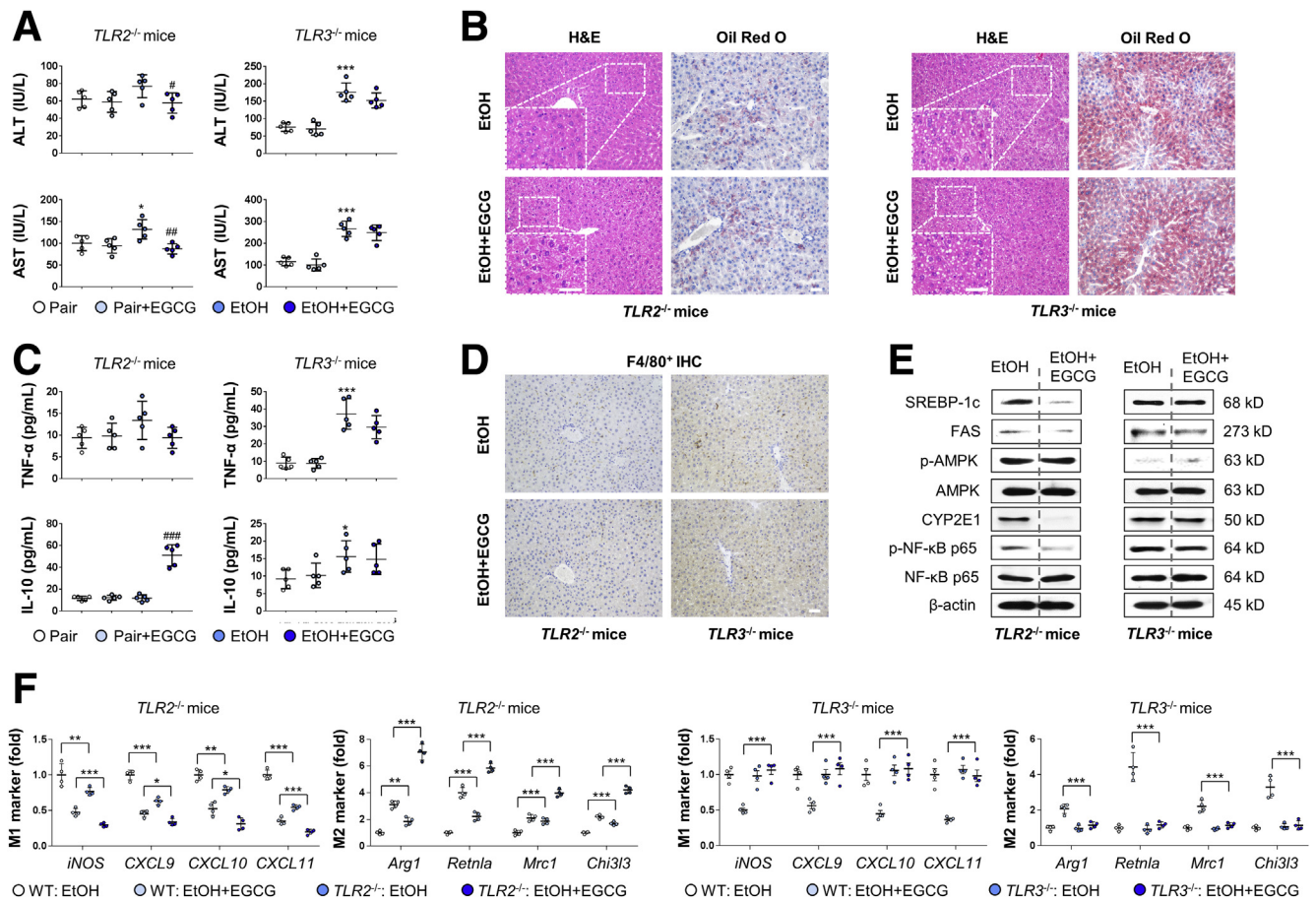
Figure 6. TLR2 and TLR3 play differential roles in EGCG-mediated ALD protection. (*A*) Serum chemistry for ALT and AST of $Tlr2^{-/-}$ and $Tlr3^{-/-}$ mice (n = 5). (*B*) Representative hepatic hematoxylin and eosin and Oil Red O staining of $Tlr2^{-/-}$ and $Tlr3^{-/-}$ mice. (*C*) Serum levels of cytokines measured by using enzyme-linked immunosorbent assay (n = 5). (*D*) Representative hepatic F4/80[+] cell staining results of $Tlr2^{-/-}$ and $Tlr3^{-/-}$ mice. (*E*) Whole liver tissue immunoblotting results of $Tlr2^{-/-}$ and $Tlr3^{-/-}$ mice. (*F*) Real-time PCR results of key M1 and M2 markers from isolated Kupffer cells from $Tlr2^{-/-}$ and $Tlr3^{-/-}$ mice treated with ethanol diet or EGCG (n = 4). Scale bar = 20 μm. Values are expressed as mean ± SD (Three independently repeated experiments with similar results). *, ***P < .05 and .001 against pair group; #, ##, ###P < .01, .05, and .001 against EtOH (ALD) group. For panel *F*: *, **, ***P < .05, .01, and .001 between indicated groups. Statistical comparisons between groups were done by using the Kruskal-Wallis test followed by Dunn's post hoc test to detect differences in all groups.

Kupffer cell TLR2 and TLR3 had divergent roles in ALD, as ablation of TLR2 ameliorated whereas TLR3 deficiency aggravated ALD phenotypes. A reduction in the synthesis and secretion of IL-10 differentially mediated by the TLRs under chronic binge seemed to drive ALD progression. Importantly, we also identified EGCG as a novel hepatoprotectant against ALD. EGCG directly interacts with KC TLR2/3 and restored IL-10 production to achieve liver protection. We have summarized these findings in a scheme to conceptually depict the potential mechanisms underlying the roles of TLR2/3 in Kupffer cell dysfunction and how EGCG intervention operates in ALD-associated liver injury (Figure 10).

In light of the pathological hallmark of alcoholic hepatitis that the disease is often associated with a faster progression to cirrhosis and liver failure than other kinds of hepatitis, well-controlled clinical management is important for those patients.[18,19] Unfortunately, abstinence and nutritional support are the only definitive clinical strategies for ALD therapy. Although multiple attempts have been made to improve ALD patients' treatment outcome, only corticosteroids regimens have been recommended in the AASLD (American Association for the Study of Liver Diseases) and EASL (European Association for the Study of the Liver) guidelines for treating severe alcoholic hepatitis.[20] Other targeted ALD treatments (eg, antioxidants or stem cells) are only in their infancy. Based on our findings here, we posit that EGCG, a major active ingredient from green tea, can efficaciously and safely ameliorate ALD-induced hepatic steatosis, inflammation, apoptosis, and Kupffer cell activation. More importantly, EGCG seems in many ways superior in ALD amelioration to other commonly used agents, such as NAC, silibinin, resveratrol, and prednisolone (Figure 2).

A major challenge in the mechanistic study on a novel ingredient from natural product is the establishment of direct target on or within the cell. Remarkably, previous
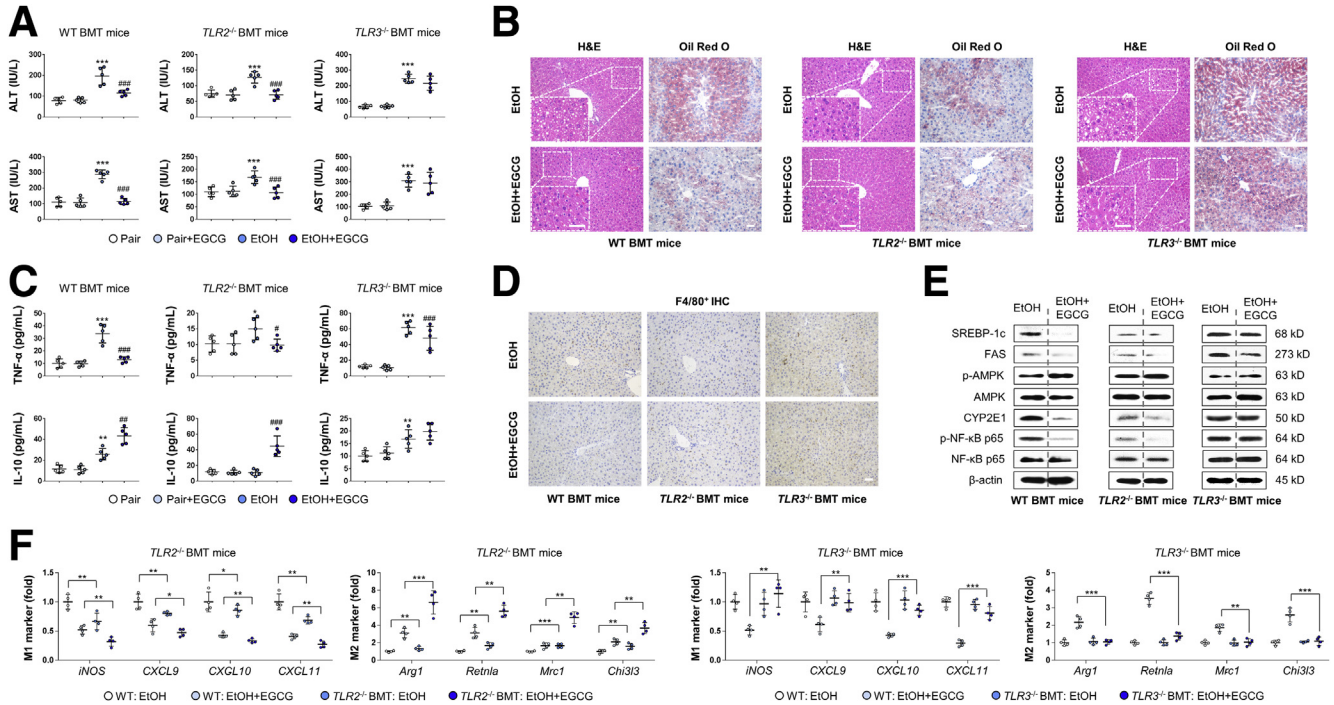
Figure 7. Kupffer cell TLR2 and TLR3 act differentially in ALD progression and EGCG protection through IL-10.
(*A*) Serum chemistry for ALT and AST of WT, *Tlr2*$^{-/-}$ and *Tlr3*$^{-/-}$ BMT mice (n = 5). (*B*) Representative hepatic hematoxylin and eosin and Oil Red O staining of WT, *Tlr2*$^{-/-}$ BMT, and *Tlr3*$^{-/-}$ BMT mice. (*C*) Serum levels of cytokines measured by using enzyme-linked immunosorbent assay (n = 5). (*D*) Representative hepatic F4/80^{+} cell staining of WT, *Tlr2*$^{-/-}$ BMT, and *Tlr3*$^{-/-}$ BMT mice. (*E*) Whole liver tissue immunoblotting results of WT, *Tlr2*$^{-/-}$ BMT, and *Tlr3*$^{-/-}$ BMT mice. (*F*) Real-time PCR results of key M1 and M2 markers from isolated Kupffer cells from WT, *Tlr2*$^{-/-}$ BMT, and *Tlr3*$^{-/-}$ BMT mice treated with ethanol diet or EGCG (n = 4). Scale bar = 20 μm. Values are expressed as mean ± SD (3 independently repeated experiments with similar results). *, **, ***P < .05, .01, and .001 against pair group; #, ##, ###*P* < .01, .05, and .001 against EtOH (ALD) group. For panel *F*: *, **, ***P < .05, .01, and .001 between indicated groups. Statistical comparisons between groups were done by using the Kruskal-Wallis test followed by Dunn's post hoc test to detect differences in all groups.

study has confirmed that EGCG could directly regulate cell surface growth factor receptors (eg, epidermal growth factor receptor) to influence cell survival, proliferation, and angiogenesis.[21] In cancer cells, a metastasis-associated laminin receptor (67LR) has been identified to confer EGCG responsiveness to cancer cells. Following studies also found that EGCG physically interacted with the ligand-binding domain of androgen receptor of prostate cancer cell.[22] Another role of EGCG-stimulated 67LR was to attenuate LPS-induced inflammation, such as to inhibit TLR4 through the action of tollip.[23] As the health-promoting properties of EGCG seem to be manifested at multiorgan levels, more direct cell surface targets are yet to be elucidated.

Several studies have confirmed the critical roles of Kupffer cells in responding to increased gut-derived endotoxins, through TLR4/NF-κB–mediated local production of proinflammatory cytokines and chemokines (eg, TNF-α, IL-6, MCP-1).[24–28] However, functions of other TLRs during ALD progression and drug therapy remain largely unknown. Our biophysical results suggest that the direct interactions between EGCG and TLR2 was relatively strong, while that between EGCG and TLR3 was intermediate. In consistent

with the previous finding, there was a negligible physical interaction between EGCG and TLR4, possible through 67LR or other signaling molecules. More importantly, TLR2 and TLR3 in Kupffer cells exerted opposite functions during ALD development because both *Tlr2*$^{-/-}$ and *Tlr2*$^{-/-}$ BMT mice exhibited improved body damage while both *Tlr3*$^{-/-}$ and *Tlr3*$^{-/-}$ BMT mice aggravated ALD-induced injury. A previous study demonstrated that *Tlr2* deficiency improved ALD-induced liver injury through the inhibition of CXCL1 and neutrophil infiltration.[10] Another study unveiled the protective role of TLR3 during ALD progression by IL-10 induction.[11] We firstly proved that Kupffer cell-specific TLR2 and TLR3 directly received signals from EGCG to differentially regulate downstream MAPK/NF-κB activation and IL-10 production (possibly via STAT3 activation). KO of either systemic or macrophage *Tlr3* or systemic *IL-10* drastically impaired the ameliorative effects of EGCG on ALD, indicating the indispensable roles of this axis in drug-mediated liver protection. Indeed, as TLR2 and TLR3 are the direct targets of EGCG, those receptors from other local cell types (eg, hepatic stellate cells) may also contribute to EGCG-mediated alleviation. For example, hepatic TLR2 was involved in quercetin-induced fibrosis inhibition. For TLR3, it is
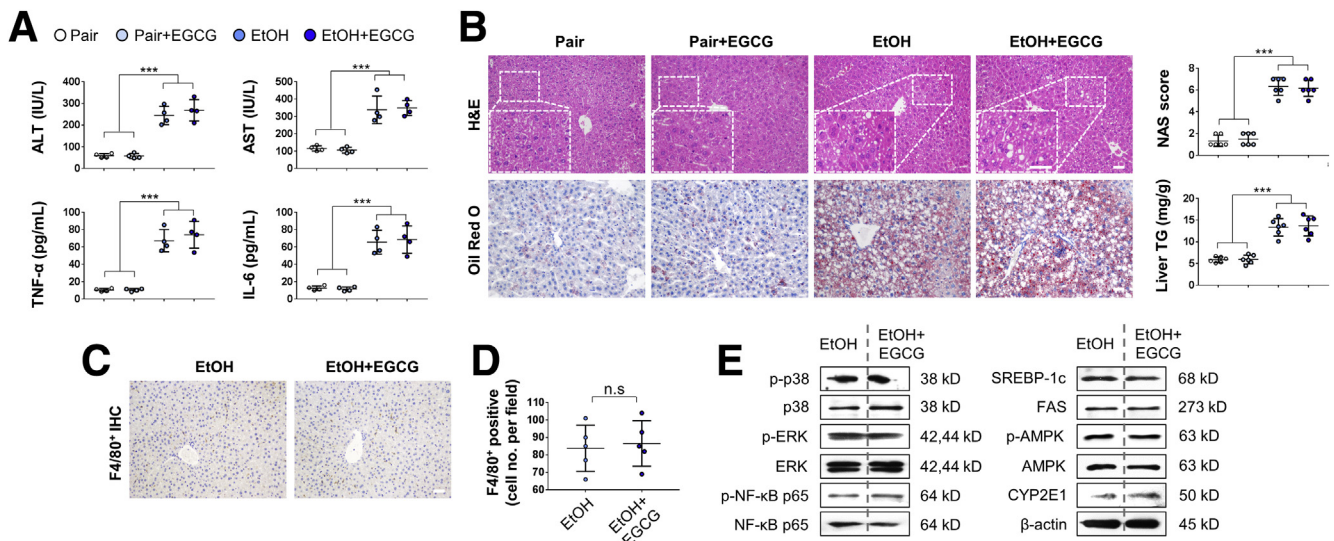
Figure 8. Deficiency of IL-10 abolished EGCG-induced hepatoprotection against ethanol-induced injury. Results of (*A*) serum chemistry (ALT and AST) (n = 4); (*B*) representative hepatic H&E/Oil Red O staining, NAS score, liver TG level (n = 6); (*C*) representative hepatic F4/80 immunohistochemistry; (*D*) F4/80 staining quantification (n = 4); and (*E*) protein markers of hepatic injury of *IL-10$^{-/-}$* mice administered with ethanol diet, in the presence or absence of EGCG. Values are expressed as mean ± SD (3 independently repeated experiments with similar results). ***$P < .001$. Scale bar = 20 μm. Statistical comparisons between groups were done by using the Kruskal-Wallis test followed by Dunn's post hoc test to detect differences in all groups. n.s., not significant.

reported that TLR3 from hepatic stellate cell (HSC) was important for IL-10 production during ALD development.[11] Moreover, IL-10 is broadly and predominantly expressed by many immune cells (most from Kupffer cells and infiltrated monocytes in the liver), and TLR2/3 provoke IL-10 production via p38 MAPK, ERK1/2, and NF-κB regulation,[29] the precise balance between mitogen- and stress-activated protein kinase 1/2 and TIR-domain-containing adaptor protein inducing interferon β pathway in the downstream of TLR2 and TLR3, respectively, may partially explain their similar IL-10 promoting effects but opposing involving roles in ALD pathogenesis.[29-31]

In conclusion, our data suggest that EGCG potently and safely ameliorates alcoholic liver injury in a murine model of ALD through TLR2/3-mediated IL-10 production. Moreover, TLR2 and TLR3 in Kupffer cells play opposite roles in EGCG-mediated protection. Thus, inhibition of TLR2 and activation of TLR3 by natural products (eg, EGCG) may constitute novel therapeutic strategies for ALD.

Materials and Methods
Chemicals and Reagents

Pure ethanol was purchased from Guangzhou Chemical Reagent Factory (Guangzhou, China). EGCG (>95% purity) was a product of Sigma-Aldrich (Cat. No. E4143) (St. Louis, MO). All cell culture consumables and reagents were supplied by either Corning Incorporated (Corning, NY) or Gibco (Carlsbad, CA). Primary antibodies against sterol regulatory element-binding protein 1c (Cat. No. ab28481), fatty acid synthase (Cat. No. ab 22759), phosphorylated adenosine AMPK at Thr172 (Cat. No. ab23875), total AMPK (Cat. No. ab32047), phosphorylated STAT3 at Tyr705 (Cat. No.

ab76315), total STAT3 (Cat. No. ab68153), NF-κB p65 at Ser536 (Cat. No. ab86299), total NF-κB p65 (Cat. No. ab16502), phosphorylated p38 MAPK at Thr180/Tyr182 (Cat. No. ab4822), total p38 MAPK (Cat. No. ab31828), phosphorylated ERK at Thr202/Tyr204 (Cat. No. ab214362), total ERK (Cat. No. ab17942), F4/80 (Cat. No. ab6640), IL-10 (Cat No. ab189392), iNOS (Cat. No. ab178945), CD206 (Cat. No. ab64693), cytochrome P450 2E1 (Cat. No. ab28146), cleaved caspase-3 (Cat. No. ab2302), cytochrome c (Cat. No. ab133504), Fas-associated death domain (Cat. No. ab124812), TLR2 (Cat. No. ab209217), TLR3 (Cat. No. ab62566), and β-actin (Cat. No. ab115777) were purchased from Abcam (Cambridge, United Kingdom).

Animals and Experimental Design

Male C57BL/6 WT mice (8 weeks old; 18–21 g) were purchased from Guangdong Medical Animal Center (Guangzhou, China). *Tlr2* KO (*Tlr2$^{-/-}$*; Cat. No. 022507), *Tlr3$^{-/-}$* (Cat. No. 029248), and *IL-10$^{-/-}$* (Cat. No. 002251) mice were ordered from the Jackson Laboratory (Bar Harbor, ME), were backcrossed to the B6 strain for more than 6 generations.. Alcoholic liver injury was induced by using the NIAAA model with minor modifications.[32] Mice were initially fed ad libitum with the control Lieber-DeCarli diet for 5 days to allow acclimation to liquid diet and tube feeding. Then, the ALD groups (chronic-binge ethanol-fed group) were fed with the Lieber-DeCarli diet containing 5% (v/v) ethanol for 10 days (the first stage), while the control mice were pair-fed with the isocaloric control diet (the same caloric content) for 10 days. Changes in body weight and food intake of each mouse were recorded every day. At day 11, ethanol-fed and pair-fed mice are gavaged in
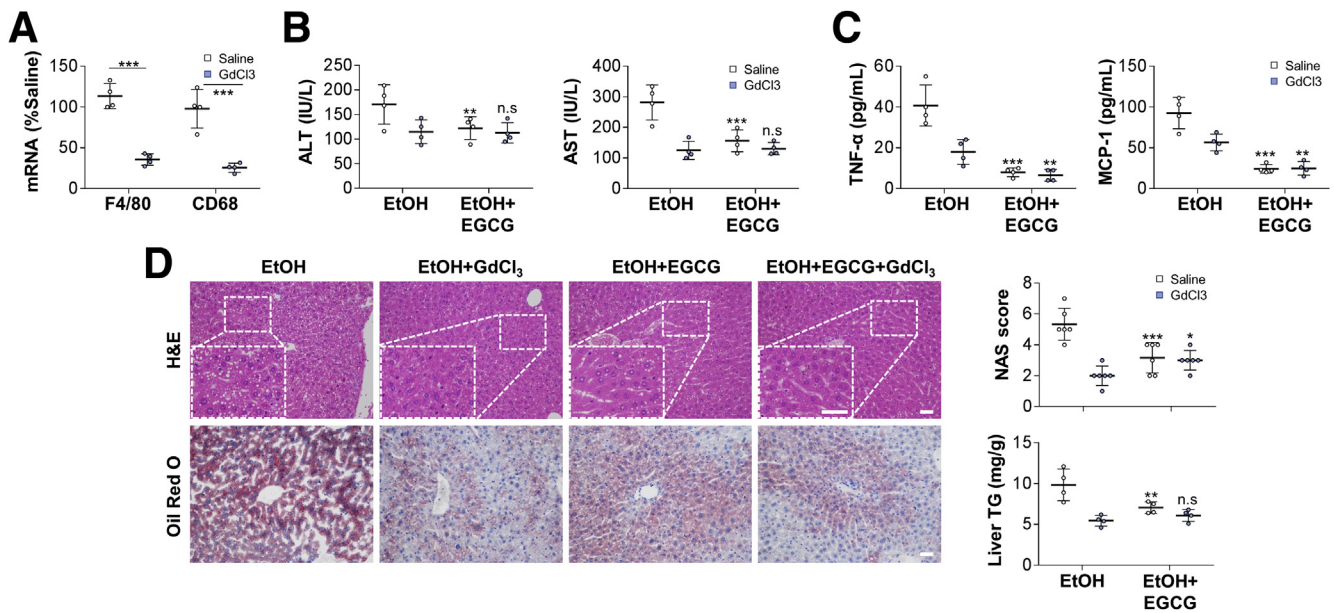
Figure 9. Depletion of Kupffer cells by GdCl₃ pretreatment improves ALD-induced hepatic injury and significantly impairs EGCG-mediated hepatoprotection. (A) Verification of Kupffer cell depletion after GdCl₃ injection by measuring messenger RNA level changes of F4/80 and CD68 (n = 4). Results of (B, C) serum chemistry (ALT and AST) (n = 4); (D) representative hepatic H&E/Oil Red O staining, NAS score (n = 5), and liver TG level (n = 4) of GdCl₃-treated mice administered with ethanol consumption in the presence or absence of EGCG. Values are expressed as mean ± SD (3 independently repeated experiments with similar results). *,**, ***P < .05, .01, and .001 same color between EtOH and EtOH+EGCG groups For panel A: ***P < .001 between indicated groups. Scale bar = 20 μm. Statistical comparisons between groups were done by using the Kruskal-Wallis test followed by Dunn's post hoc test to detect differences in all groups.

the early morning (∼8:00 AM) with a single dose of ethanol (the binge consumption; 5 g/kg body weight) or isocaloric maltose dextrin, respectively, and euthanized 9 hours later by using 150 mg/kg pentobarbital (intraperitoneal injection). For the experiments with $IL-10^{-/-}$ mice, the ethanol treatment doses (during the 10-day period) were adjusted to 3% (v/v) for the first stage and 3 g/kg for the binge stage, because of the increased sensitivity to alcohol of $IL-10^{-/-}$ mice. EGCG (50 mg/kg, in normal saline) regimens by gavaging were started when they at day 6 and administered every day.[5] Pair-fed mice were gavaged with the same volume of saline. Parallel experiments using resveratrol (0.0125% v/v mixed in total diet) (Sigma-Aldrich, Cat. No. R5010),[33] silibinin (Legalon SIL, 25 mg/kg, intraperitoneal injection, every other day) (Sigma-Aldrich, Cat. No. 02000585),[34] NAC (100 mg/kg, gavage, every other day) (Sigma-Aldrich, Cat. No. BP907),[35] and prednisolone (10 mg/kg/day, gavage, every other day) (Sigma-Aldrich, Cat. No. BP464)[36] were also conducted using the same NIAAA model. For bone marrow transplantation, whole bone marrow was prepared from wild-type, $Tlr2^{-/-}$, $Tlr3^{-/-}$, and $IL-10^{-/-}$ mice and injected intravenously (5 × 10⁶ cells/recipient) into lethally irradiated (850 rad) WT recipients. Transplant recipient mice were kept for 3 weeks for bone
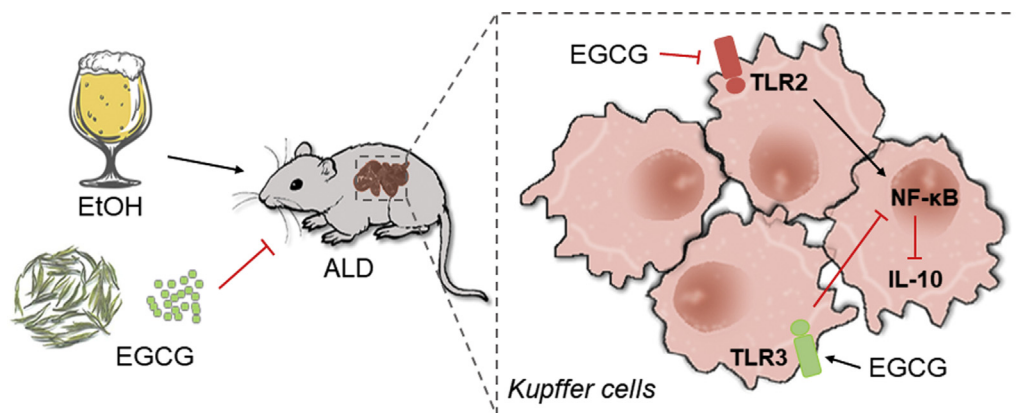

Figure 10. A model depicting the mechanism by which EGCG alleviates ALD-induced hepatic injury through divergent regulations of Kupffer cell TLR2 and TLR3.

Table 1. Primer Sequence Information for Quantitative Real-Time Polymerase Chain Reaction assay

Target gene	Direction	Primer sequence (5'-3')	A. Temp. (°C)
Arg1	Forward Reverse	CTCCAAGCCAAAGTCCTTAGAG AGGAGCTGTCATTAGGGACATC	56
CD68	Forward Reverse	TGTCTGATCTTGCTAGGACCG GAGAGTAACGGCCTTTTTGTGA	56
Chi3l3	Forward Reverse	CAGGTCTGGCAATTCTTCTGAA GTCTTGCTCATGTGTGTAAGTGA	56
CXCL9	Forward Reverse	TCCTTTTGGGCATCATCTTCC TTTGTAGTGGATCGTGCCTCG	56
CXCL10	Forward Reverse	CCAAGTGCTGCCGTCATTTTC GGCTCGCAGGGATGATTTCAA	58
CXCL11	Forward Reverse	GGCTTCCTTATGTTCAAACAGGG GCCGTTACTCGGGTAAATTACA	56
F4/80	Forward Reverse	GAGATTGTGGAAGCATCCGAGAC GATGACTGTACCCACATGGCTGA	57
GAPDH	Forward Reverse	CTGGGCTACACTGAGCACC AAGTGGTCGTTGAGGGCAATG	58
IL-10	Forward Reverse	GCTCTTACTGACTGGCATGAG CGCAGCTCTAGGAGCATGTG	56
iNOS	Forward Reverse	GGAGTGACGGCAAACATGACT TCGATGCACAACTGGGTGAAC	56
Mrc1	Forward Reverse	CTCTGTTCAGCTATTGGACGC CGGAATTTCTGGGATTCAGCTTC	58
Retnla	Forward Reverse	CCAATCCAGCTAACTATCCCTCC ACCCAGTAGCAGTCATCCCA	56

A. Temp., Annealing temperature

marrow reconstitution and were then used to establish the NIAAA model as described previously. To deplete Kupffer cells from murine liver, mice received an intraperitoneal injection of either 0.9% NaCl (5 mL/kg, Sigma-Aldrich, Cat. No. 52455) or GdCl3 (20 mg/kg, Sigma-Aldrich, Cat. No. 721905) twice a week, 1 week before the start, and throughout the entire period of NIAAA modeling. All experimental procedures were approved by the Ethical Committee of Shenzhen Third People's Hospital.

Serum/Hepatic Biochemistry and Cytokine Measurements

Serum ALT, AST, TG, and TC were measured using Hitachi LABOSPECT 008 (Hitachi High-Tech Co, Tokyo, Japan). Serum and hepatic cytokine protein levels were determined by using corresponding enzyme-linked immunosorbent assay kits from Peprotech (Rocky Hill, NJ) according to manufacturer's instructions: TNF-α (Cat. No. 900-M54), MCP-1 (Cat. No. 900-M126), IL-10 (Cat. No. 900-M53), IL-1β (Cat. No. 900-M47), and IL-6 (Cat. No. 900-M50). Total contents of hepatic TG were measured by a colorimetric TG assay kit from Sigma-Aldrich (Cat. No. MAK266-1KT).

Isolation of Mononuclear Cells, Kupffer Cells, HSCs, and In Vitro Treatments

Total liver mononuclear cells (MNCs) were isolated as previously described.[11] In detail, liver tissues were homogenized and filtered through a 70-μm cell strainer

(BD Biosciences, San Jose, CA). Then cell suspension was centrifuged at 400 rpm for 5 minutes at room temperature to eliminate hepatocytes. After that, the supernatant was further subjected to 40% Percoll resuspension and gently overlaid onto 70% Percoll for a 25-minute centrifugation at 2500 rpm. Isolation of Kupffer cells and HSCs from mice was performed as previously described.[37] That is, 2-step perfusion was performed by using 60 mg/dL Pronase E (Roche Applied Science, Penzberg, Germany) solution in Hanks' Balanced Salt Solution (HBSS) (Sigma-Aldrich) with calcium and magnesium followed by a solution of 60 mg/dL collagenase D. Mouse livers ($n = 1$–3 mice) were minced in a Petri dish and incubated at 37°C by constant shaking in a solution containing 50 mg/dL Pronase, 50-mg/dL collagenase D, and 20-μg/dL DNase I (all from Roche Applied Science) in HBSS containing calcium and magnesium. Livers were then filtered through a sterile nylon mesh and entrapped cells were washed twice with HBSS containing calcium and magnesium, followed by discontinuous density gradient centrifugation with a 2-layer Nycodenz (Axis-shield, Oslo, Norway). Cells in the top layer were 95% HSCs, as judged by retinoid auto-fluorescence and contained <3% CD11b- or CD146-positive cells. The pelleted cells were washed twice and were used for fluorescence-activated cell sorting (FACS) In a Dako Cytomation (now Beckman-Coulter, Brea, CA) MoFloT High-Performance Cell Sorter with the SummitT software program, with PE-conjugated antibodies against CD11b (Cat. No. 101215, clone M1/70) (BioLegend, San

Table 2. Composition Changes of Liver Mononuclear Cells in WT Mice After Ethanol or EGCG Treatments

Population	Pair (n = 6)	Pair+EGCG (n = 6)	EtOH (n = 6)	EtOH+EGCG (n = 6)	P value[a]
Macrophages (F4/80$^+$CD11b$^+$)	5.15 ± 1.28%	5.10 ± 1.07%	9.85 ± 2.55%	5.93 ± 1.99%	.02
NK cells (CD3$^-$NK1.1$^+$)	15.48 ± 3.27%	15.65 ± 3.14%	8.40 ± 2.46%	13.83 ± 4.31%	.03
NKT cells (CD3$^+$NK1.1$^+$)	23.92 ± 5.54%	24.51 ± 5.00%	17.80 ± 4.45%	23.65 ± 3.51%	.04
CD4 T cells (CD3$^+$CD4$^+$)	33.78 ± 4.72%	31.83 ± 4.57%	29.35 ± 5.70%	33.88 ± 6.21%	.26
CD8 T cells (CD3$^+$CD8$^+$)	16.20 ± 2.54%	15.18 ± 4.49%	14.05 ± 3.62%	16.25 ± 4.02%	.38
Granulocytes (Gr1$^+$CD11b$^+$)	13.78 ± 3.18%	14.20 ± 3.31%	11.85 ± 3.93%	13.93 ± 6.07%	.53

Values are mean ± SD. n = 4 (experiments were independently repeated 3 times).
EGCG, epigallocatechin-3-gallate; EtOH, ethanol; NK, natural killer; NKT, natural killer T; WT, wild-type.
[a]Between the EtOH and EtOH+EGCG groups.

Diego, CA) for Kupffer cells and CD146 (Cat. No. 134713, clone ME-9F1) (BioLegend) for liver sinusoidal endothelial cells (LSECs), respectively, yielding > 95% purity. All cells were cultured on uncoated plastic tissue culture dishes in Dulbecco's modified Eagle medium containing 10% fetal bovine serum and used as nonpassaged primary cultures only.

To measure the effects of ethanol and EGCG on liver MNC composition, isolated MNCs were stained with anti-F4/80 (BM8, Cat. No. 123115/123109), anti-CD45 (30-F11, Cat. No. 103111/103105), anti-CD11b (M1/70, Cat. No. 101207/101211) (all from BioLegend), anti-CD3e (145-2C11, Cat. No. 553061), anti-NK1.1 (PK136, Cat. No. 553164/550627), anti-CD4 (RM4-5, Cat. No. 553051/553046), and anti-Gr1 (RB6-8C5, Cat. No. 553126/553128) (all from BD Biosciences) for FACS analysis.

To acquire conditioned medium from polarized isolated Kupffer cells, cells were firstly serum-starved for 24 hours and then stimulated with 1-ng/mL LPS (Sigma-Aldrich, Cat. No. L2630), 5-ng/mL recombinant human IL-4 (Sigma-Aldrich, Cat. No. IL004), or 50-μg/mL EGCG or vehicle for another 24 hours. Conditioned media were centrifuged to remove cell debris, and incubated with mouse AML-12 cells (ATCC, Cat. No. CRL-2254) for an additional 12-hour period. Hepatocytes were then incubated with 10% formalin (Sigma-Aldrich, Cat. No. HT5011) for 70 minutes and 60% isopropanol (Sigma-Aldrich, Cat. No. 19516) for 5 minutes, stained with fresh Oil Red O for 10 minutes, rinsed switch and counterstained with hematoxylin. Quantification of Oil Red O staining was performed with the ImageJ software (Version 1.8.0 National Institutes of Health, Bethesda, MD).

Histology of Liver Tissues

After sacrifice, liver tissues from all mice were fixed in 10% phosphate-buffered formalin and embedded in paraffin blocks. Tissue sections (5 μm) were cut and stained with hematoxylin and eosin, Sirius red, and Oil Red O (Sigma-Aldrich) for histological analysis using a LEICA Qwin Image Analyser (Leica Microsystems Ltd, Milton Keynes, United Kingdom). The nonalcoholic fatty liver disease activity score (NAS) of each group was calculated as previously described (ie, a sum of steatosis grade from 0 to 3, lobular inflammation from 0 to 3, and liver cell ballooning from 0 to 2).[38] Immunohistochemistry of F4/80 was performed as we reported previously.[39] That is, sodium citrate 10 mM, pH 6.0 (Sigma-Aldrich, Cat. No. 1613859) was used to peform the heat-induced antigen retreval step for embedded liver tissue sections. The concentration of F4/80 primary antibody used here was 10 μg/mL diluted in Tris-buffered saline (TBS) with 1% bovine serum albumin (all from Sigma-Aldrich). Horseradish peroxidase (HRP) conjugate goat anti-rat secondary antibody (Abcam, Cat. No. ab7097) was used to show the IHC signal.

Caspase-3/7 Activity Assay

Activities of caspases-3/7 from cell lysates after treatments were measured using Cell Meter Caspase 3/7 Activity Apoptosis Assay Kit (Cat. No. 22797) (AAT Bio, Sunnyvale, CA) according to the user manual. Final results were read at 520 nm in a microplate reader (Bio-Rad, Hercules, CA) and expressed as fold change in caspase-3/7 activity relative to the control.

Immunofluorescence Staining

Liver tissues were frozen and cryo-sectioned for immunofluorescence staining. For cell staining, cells were grown as monolayers on coverslips and exposed to each indicated treatment. Cells were washed with phosphate buffered saline and fixed with 4% paraformaldehyde for 15 minutes at room temperature. Subsequently, cells were permeabilized in 0.5% Triton solution for 2 minutes at room temperature. Primary antibodies against F4/80, IL-10, CD206, and iNOS (Abcam) (1–5 μg/mL) were incubated overnight at 4°C. Secondary fluorescein-conjugated antibodies (all from Abcam) (for F4/80 and IL-10: Cat. No. 150165; for CD206 and iNOS: Cat. No. ab150075) were then added for incubation (60 minutes). Nuclei were counterstained with DAPI) (Sigma-Aldrich; Cat. No. D8417). Control experiments omitting one of the primary antibodies but reproducing the entire staining procedure was carried out to ensure the specificity of immunostaining.

Quantitative Real-Time Polymerase Chain Reaction

Total RNA was extracted from cells, fresh liver tissue samples or cell lysates by using the CellAmp Direct RNA Prep Kit (Takara Bio Inc., Shiga, Japan; Cat. No. 3732). The first strand cDNA was synthesized from total RNA using a PrimeScript RT reagent Kit (Takara, Cat. No. RR037B) following the manufacturer's instructions. Quantitative real-time polymerase chain reaction (PCR) was performed with the sybr premix Taq Quantitative PCR Kit (Takara) (Cat. No. R004A) according to the manufacturer's instructions, on a MyiQ2 real-time quantitative PCR machine (Bio-Rad). Primer information is as listed in Table 1. Glyceraldehyde-3-phosphate dehydrogenase was amplified as an internal control. The relative quantification of messenger RNA expression levels was done according to the $2^{-\triangle\triangle Ct}$ method. All real-time PCR procedures, including the design of primers, validation of PCR environment and quantification methods, were performed according the MIQE guideline.[40]

Protein Extraction and Western Blot

After treatments, cells or liver tissues were washed with sterile phosphate-buffered saline for 3 times and then subjected to total protein extraction by using an radio-immunoprecipitation assay (RIPA) kit from Sigma-Aldrich (Cat. No. R0278). For secreted protein, culture media were collected and centrifuged for RIPA extraction. Then protein samples were quantified with bicinchoninic acid assay (BCA) reagent from Bio-Rad (Cat. No. 5000001). Western blot analyses of all proteins were performed as described using β-actin as the internal control.

Preparation of Recombinant Mouse Proteins

Full-length mouse *Tlr2/3/4/9* genes (NCBI IDs: 24088, 142980, 21898, and 81897, respectively) were synthesized by Shanghai Integrated Biotech Solutions Co Ltd (Shanghai, China). These genes, fused with 6 His tags at their C-termini, were subcloned into the frame of the pFastbac1 vector (Cat. No. 10360014) (Invitrogen, Waltham, MA) using the EcoRI and XhoI restriction sites. Then plasmids were transformed into DH10Bac competent cells (Invitrogen, Cat. No. 10361012), and the recombinant bacmid DNA was isolated and verified according to the Bac-to-Bac Baculovirus Expression System instructions (Invitrogen). Sf9 insect cells were then transfected to generate recombinant baculovirus, and the titer of the baculoviral stock was amplified by infecting the Sf9 insect cells with P1 and P2 viral stocks.

For purification, the culture medium from the insect cells that contained the target protein was first centrifuged at 12000 rpm at 4°C for 30 minutes to remove the cells and cell debris, and was then loaded onto HiTrap Ni Fast Flow beads (GE Healthcare, Madison, WI) that were previously equilibrated with 50 mM phosphate-buffered saline (50-mM Na_2HPO_4, 10-mM KH_2PO_4, 137-mM NaCl, and 2.7-mM KCl, pH 7.4) at 4°C. The beads were sequentially washed using 50 mM phosphate-buffered saline containing first 20-mM and then 50-mM imidazole. They were then eluted with 50 mM phosphate-buffered saline supplemented with 300-mM imidazole. The protein was further purified on a size exclusion chromatography (SEC) column that was equilibrated with 20-mM HEPES, pH 7.5, and 150-mM NaCl. The pooled peak fractions (pH 7.5) were concentrated to 13 mg/mL, and aliquots were flash-frozen in liquid nitrogen and stored at –80°C until further use.

SPR and Thermal Shift Assay

Analysis of direct interactions between EGCG and TLR2/3/4/9 proteins was performed at 25°C on a BIAcore T100 SPR instrument (GE Healthcare). SPR running buffer contained 50-mM HEPES (pH 7.5), 150-mM NaCl, 3-mM EDTA, and 0.005% (v/v) Tween 20 and was prepared immediately before measurement. BIAcore sensor chip CM5 (Cat. No. 29104988) was activated for 5–10 minutes in a 1:1 mixture of 0.1-M N-hydroxysuccinimide and 0.1-M *N*-ethyl-*N′*-(3-diethylaminopropyl)-carbodiimideat a flow rate of 10 μL/min. Recombinant mouse protein was immobilized via amine coupling on a flow cell of the chip. The remaining binding sites on the chips were blocked by 1-M ethanolamine (pH 8.5) at a flow rate of 10 μL/min for 5 minutes. Control sensorgrams, obtained on an empty flow cell where the coupling reaction had been conducted in the presence of coupling buffer alone, were always subtracted from binding responses. EGCG was diluted in the running buffer and then injected at different concentrations (100, 200, and 400 μg/mL) and passed over adjacent target and control flow cells at a flow rate of 20 μL/min for 180 seconds. After a 5-minute dissociation, the bound analytes were removed by a 20-second wash with 20-mM NaOH.

For TSA, we used 0.04 mg/mL of recombinant receptor protein with or without 0.2 mM of EGCG in phosphate-buffered saline. Data were analyzed with the differential scanning fluorimetry analysis tool (Excel based) using the curve-fitting software XLfit 5 (ID Business Solutions Ltd, Guildford, United Kingdom).[41]

Protein Structure Modeling

TLR3 is unique since it binds a form of nucleic acid called double-strand RNA. We investigated interactions between TLR3 and EGCG by molecular docking analysis. The mouse TLR3 structure was retrieved from the Protein Data Bank database (code: 3CIY). The structure of TLR3 was refined, including removing all water molecules, nonbonded heteroatoms, and adding missing hydrogen atoms by UCSF Chimera program (http://www.cgl.ucsf.edu/chimera/). Then, the binding pose of EGCG in the active binding site of TLR3 was predicted by the AutoDock software (version 4.2.6). The TLR3 and EGCG were prepared by AutoDockTools software (version 1.5.6).

Statistical Analysis

Data from each group are expressed as mean ± SD. Statistical comparisons between groups were done by using

the Kruskal-Wallis test followed by Dunn's post hoc test to detect differences in all groups. Statistical significance was determined at $P < .05$ (Prism 5.0, GraphPad Software, San Diego, CA).

References

1. Lucey MR, Mathurin P, Morgan TR. Alcoholic hepatitis. N Engl J Med 2009;360:2758–2769.

2. Lanthier N, Starkel P. Treatment of severe alcoholic hepatitis: past, present and future. Eur J Clin Invest 2017; 47:531–539.

3. McCabe MEt, Siddique A, Kowdley KV. ACP Journal Club. Adding N-acetylcysteine to prednisolone reduced early mortality in severe alcoholic hepatitis. Ann Intern Med 2012;156:JC5-5.

4. Nguyen-Khac E, Thevenot T, Piquet MA, Benferhat S, Goria O, Chatelain D, Tramier B, Dewaele F, Ghrib S, Rudler M, Carbonell N, Tossou H, Bental A, Bernard-Chabert B, Dupas JL. Glucocorticoids plus N-acetylcysteine in severe alcoholic hepatitis. N Engl J Med 2011;365:1781–1789.

5. Huang L, Xu H, Peng G. TLR-mediated metabolic reprogramming in the tumor microenvironment: potential novel strategies for cancer immunotherapy. Cell Mol Immunol 2018;15:428–437.

6. Mandal P, Roychowdhury S, Park PH, Pratt BT, Roger T, Nagy LE. Adiponectin and heme oxygenase-1 suppress TLR4/MyD88-independent signaling in rat Kupffer cells and in mice after chronic ethanol exposure. J Immunol 2010;185:4928–4937.

7. Petrasek J, Bala S, Csak T, Lippai D, Kodys K, Menashy V, Barrieau M, Min SY, Kurt-Jones EA, Szabo G. IL-1 receptor antagonist ameliorates inflammasome-dependent alcoholic steatohepatitis in mice. J Clin Invest 2012;122:3476–3489.

8. Gustot T, Lemmers A, Moreno C, Nagy N, Quertinmont E, Nicaise C, Franchimont D, Louis H, Deviere J, Le Moine O. Differential liver sensitization to toll-like receptor pathways in mice with alcoholic fatty liver. Hepatology 2006;43:989–1000.

9. Hritz I, Mandrekar P, Velayudham A, Catalano D, Dolganiuc A, Kodys K, Kurt-Jones E, Szabo G. The critical role of toll-like receptor (TLR) 4 in alcoholic liver disease is independent of the common TLR adapter MyD88. Hepatology 2008;48:1224–1231.

10. Roh YS, Zhang B, Loomba R, Seki E. TLR2 and TLR9 contribute to alcohol-mediated liver injury through induction of CXCL1 and neutrophil infiltration. Am J Physiol Gastrointest Liver Physiol 2015; 309:G30–G41.

11. Byun JS, Suh YG, Yi HS, Lee YS, Jeong WI. Activation of toll-like receptor 3 attenuates alcoholic liver injury by stimulating Kupffer cells and stellate cells to produce interleukin-10 in mice. J Hepatol 2013; 58:342–349.

12. Xiao J, Ho CT, Liong EC, Nanji AA, Leung TM, Lau TY, Fung ML, Tipoe GL. Epigallocatechin gallate attenuates fibrosis, oxidative stress, and inflammation in non-alcoholic fatty liver disease rat model through TGF/ SMAD, PI3 K/Akt/FoxO1, and NF-kappa B pathways. Eur J Nutr 2014;53:187–199.

13. Chen C, Liu Q, Liu L, Hu YY, Feng Q. Potential biological effects of (-)-epigallocatechin-3-gallate on the treatment of nonalcoholic fatty liver disease. Mol Nutr Food Res 2018;62:201700483.

14. Santamarina AB, Carvalho-Silva M, Gomes LM, Okuda MH, Santana AA, Streck EL, Seelaender M, do Nascimento CM, Ribeiro EB, Lira FS, Oyama LM. Decaffeinated green tea extract rich in epigallocatechin-3-gallate prevents fatty liver disease by increased activities of mitochondrial respiratory chain complexes in diet-induced obesity mice. J Nutr Biochem 2015; 26:1348–1356.

15. Wang D, Gao Q, Wang T, Zhao G, Qian F, Huang J, Wang H, Zhang X, Wang Y. Green tea infusion protects against alcoholic liver injury by attenuating inflammation and regulating the PI3K/Akt/eNOS pathway in C57BL/6 mice. Food Funct 2017;8:3165–3177.

16. Park JH, Kim SJ, Hwang I, Bae KC, Bae JH, Song DK. Green tea extract co-administered with a polymer effectively prevents alcoholic liver damage by prolonged inhibition of alcohol absorption in mice. Alcohol Alcohol (Oxford, Oxfordshire) 2013;48:59–67.

17. Park JK, Shao M, Kim MY, Baik SK, Cho MY, Utsumi T, Satoh A, Ouyang X, Chung C, Iwakiri Y. An endoplasmic reticulum protein, Nogo-B, facilitates alcoholic liver disease through regulation of kupffer cell polarization. Hepatology 2017;65:1720–1734.

18. Mathurin P, Beuzin F, Louvet A, Carrie-Ganne N, Balian A, Trinchet JC, Dalsoglio D, Prevot S, Naveau S. Fibrosis progression occurs in a subgroup of heavy drinkers with typical histological features. Aliment Pharmacol Ther 2007;25:1047–1054.

19. Verrill C, Markham H, Templeton A, Carr NJ, Sheron N. Alcohol-related cirrhosis–early abstinence is a key factor in prognosis, even in the most severe cases. Addiction 2009;104:768–774.

20. Louvet A, Mathurin P. Alcoholic liver disease: mechanisms of injury and targeted treatment. Nat Rev Gastroenterol Hepatol 2015;12:231–242.

21. Kim HS, Quon MJ, Kim JA. New insights into the mechanisms of polyphenols beyond antioxidant properties; lessons from the green tea polyphenol, epigallocatechin 3-gallate. Redox Biol 2014;2:187–195.

22. Tachibana H, Koga K, Fujimura Y, Yamada K. A receptor for green tea polyphenol EGCG. Nat Struct Mol Biol 2004;11:380–381.

23. Hong Byun E, Fujimura Y, Yamada K, Tachibana H. TLR4 signaling inhibitory pathway induced by green tea polyphenol epigallocatechin-3-gallate through 67-kDa laminin receptor. J Immunol 2010;185:33–45.

24. Inokuchi S, Tsukamoto H, Park E, Liu ZX, Brenner DA, Seki E. Toll-like receptor 4 mediates alcohol-induced steatohepatitis through bone marrow-derived and endogenous liver cells in mice. Alcohol Clin Exp Res 2011;35:1509–1518.

25. Kirpich IA, Feng W, Wang Y, Liu Y, Barker DF, Barve SS, McClain CJ. The type of dietary fat modulates intestinal tight junction integrity, gut permeability, and hepatic

toll-like receptor expression in a mouse model of alcoholic liver disease. Alcohol Clin Exp Res 2012; 36:835–846.

26. Hartmann P, Chen WC, Schnabl B. The intestinal microbiome and the leaky gut as therapeutic targets in alcoholic liver disease. Front Physiol 2012;3:402.

27. Roh YS, Seki E. Toll-like receptors in alcoholic liver disease, non-alcoholic steatohepatitis and carcinogenesis. J Gastroenterol Hepatol 2013;28(Suppl 1):38–42.

28. Yang J, Yan H. TLR5: beyond the recognition of flagellin. Cell Mol Immunol 2017;14:1017–1019.

29. Saraiva M, O'Garra A. The regulation of IL-10 production by immune cells. Nat Rev Immunol 2010;10:170–181.

30. Zorde-Khvalevsky E, Abramovitch R, Barash H, Spivak-Pohis I, Rivkin L, Rachmilewitz J, Galun E, Giladi H. Toll-like receptor 3 signaling attenuates liver regeneration. Hepatology 2009;50:198–206.

31. Chang J, Kunkel SL, Chang CH. Negative regulation of MyD88-dependent signaling by IL-10 in dendritic cells. Proc Natl Acad Sci U S A 2009;106:18327–18332.

32. Bertola A, Mathews S, Ki SH, Wang H, Gao B. Mouse model of chronic and binge ethanol feeding (the NIAAA model). Nat Protoc 2013;8:627–637.

33. Ahn J, Cho I, Kim S, Kwon D, Ha T. Dietary resveratrol alters lipid metabolism-related gene expression of mice on an atherogenic diet. J Hepatol 2008; 49:1019–1028.

34. Schumann J, Prockl J, Kiemer AK, Vollmar AM, Bang R, Tiegs G. Silibinin protects mice from T cell-dependent liver injury. J Hepatol 2003;39:333–340.

35. Zeng T, Zhang CL, Zhao N, Guan MJ, Xiao M, Yang R, Zhao XL, Yu LH, Zhu ZP, Xie KQ. Impairment of Akt activity by CYP2E1 mediated oxidative stress is involved in chronic ethanol-induced fatty liver. Redox Biol 2018; 14:295–304.

36. Laskewitz AJ, van Dijk TH, Bloks VW, Reijngoud DJ, van Lierop MJ, Dokter WH, Kuipers F, Groen AK, Grefhorst A. Chronic prednisolone treatment reduces hepatic insulin sensitivity while perturbing the fed-to-fasting transition in mice. Endocrinology 2010;151:2171–2178.

37. Seki E, De Minicis S, Osterreicher CH, Kluwe J, Osawa Y, Brenner DA, Schwabe RF. TLR4 enhances TGF-beta signaling and hepatic fibrosis. Nat Med 2007; 13:1324–1332.

38. Brunt EM, Kleiner DE, Wilson LA, Belt P, Neuschwander-Tetri BA. Nonalcoholic fatty liver disease (NAFLD) activity score and the histopathologic diagnosis in NAFLD: distinct clinicopathologic meanings. Hepatology 2011; 53:810–820.

39. Xiao J, Xing F, Huo J, Fung ML, Liong EC, Ching YP, Xu A, Chang RC, So KF, Tipoe GL. Lycium barbarum polysaccharides therapeutically improve hepatic functions in non-alcoholic steatohepatitis rats and cellular steatosis model. Sci Rep 2014;4:5587.

40. Bustin SA, Benes V, Garson JA, Hellemans J, Huggett J, Kubista M, Mueller R, Nolan T, Pfaffl MW, Shipley GL, Vandesompele J, Wittwer CT. The MIQE guidelines: minimum information for publication of quantitative real-time PCR experiments. Clin Chem 2009;55:611–622.

41. Ouyang S, Song X, Wang Y, Ru H, Shaw N, Jiang Y, Niu F, Zhu Y, Qiu W, Parvatiyar K, Li Y, Zhang R, Cheng G, Liu ZJ. Structural analysis of the STING adaptor protein reveals a hydrophobic dimer interface and mode of cyclic di-GMP binding. Immunity 2012; 36:1073–1086.

Correspondence
Address correspondence to: Hua Wang, MD, PhD, Department of Oncology, the First Affiliated Hospital, Institute for Liver Diseases of Anhui Medical University, Hefei 230022, China. e-mail: wanghua@ahmu.edu.cn; fax: +86-551-65161056; or Jia Xiao, PhD, Clinical Medicine Research Institute, the First Affiliated Hospital of Jinan University, Guangzhou 510632, China. e-mail: edwinsiu@connect.hku.hk; fax: +86-20-38688000.